

background. It is very difficult to extract the direct QGP photon signal, which is only a small fraction of all photons produced.

Because dilepton formation, compared with formation of photons, requires one additional electromagnetic interaction, the yield of dileptons is considerably smaller, by a factor 300 or more, than the yield of direct photons. However, the dilepton background is also much reduced. While the directly produced photons are present at the level of 5% of the photon signal observed, the amount of dileptons from formation of dense matter is believed to exceed the background by a factor as large as 3–5. However, dileptons have been shown to have other origins related to properties of confined hadronic matter and the observed pattern of dilepton production, given the large systematic experimental error, is difficult to interpret [22]. We will not dwell on this complex subject in this book.

The diagnostic strength of the strangeness signature, in comparison with direct photons and dileptons, is that, aside from the overall enhancement of abundance, we also have the pattern of enhancement shown in Fig. 1.6, and the matter–antimatter symmetry seen in Fig. 1.7. The yield of strangeness is related to the initial most extreme conditions of the QGP phase, much like the photon and dilepton yields. However, strangeness has relatively little background. The source of strangeness, gluons, is by far more characteristic for the new phase of matter than is the source of photons and dileptons, which are electrical currents of quarks, present both in the confined and in the deconfined state of matter.

2 Hadrons

2.1 Baryons and mesons

As the above first and qualitative discussion of signals of QGP formation has shown, to pursue the subject we next need to understand rather well the properties of ‘elementary’ particles, and specifically strongly interacting (hadronic) particles. These are complex composites of the more elementary strongly interacting particles: quarks and gluons. Quark-composite hadronic particles are final products emerging from heavy-ion collisions, and play an important role in this book – there are two different types of colorless quark bound states: baryons, comprising three valence quarks, and mesons, which are quark–antiquark bound states.

Typically, each type of (composite) hadron has many resonances, i.e., states of greater mass but the same quantum number, which are generally internal structural excitations of the lowest-mass state. Normally the lowest-mass states of a given quantum number are stable (that is, if they decay, it occurs very slowly compared with the time scale of hadronic reactions), but there are notable exceptions, such as the Δ -resonances,

which are subject to the rapid hadronic decay $\Delta \rightarrow N + \pi$, which occurs within a duration less than the life span of a hadronic fireball.

On the other hand, some unstable hadronic resonances can be stable on this time scale. However, by the time relatively distant experimental detectors record a particle, all possible hadronic decays and even many weak decays have occurred. To study particles produced in high-energy nuclear collisions, we need to understand their decay patterns well.

Because the two light quarks are practically indistinguishable under strong interactions, their bound states reflect a symmetry, referred to as isospin I . In addition one is normally quoting the strange-quark content (strangeness S) of a bound hadron state. Similarly, we refer to more exotic baryons by quoting the value of their charm content C or bottom content B . It is believed that the heaviest quark t can not form hadronic bound states, since its life span is too short for a (quantum) orbit to form.

We keep in mind that, for historical reasons, strange baryons, containing strange quarks s , have *negative* strangeness (hyperon number) S , and that strange mesons, with a strange quark s , are called antikaons $\bar{K}(s\bar{q})$ (we indicate in the parentheses the valence-quark content). Similar conventions were adopted for charm and bottom flavors.

• Baryons

In Fig. 2.1, we present baryons made of the four lightest quarks (u , d , s , and c). Were all four quark flavors degenerate in mass, we would have instead of the isospin $SU(2)$ an $SU(4)$ flavor symmetry. In Fig. 2.1, the vertical hierarchy is generated by the largest symmetry breaking in the hadron mass spectrum, introduced by the relatively large mass of the charmed quark. The two ‘foundations’ of the $SU(4)$ flavor-multiplet ‘pyramids’ are the $SU(3)$ flavor multiplets, arising when three quarks (u , d , and s) are considered: in Fig. 2.1(a) a spin- $\frac{1}{2}$ ‘octet’ (eight-fold multiplicity); in Fig. 2.1(b) a spin- $\frac{3}{2}$ ‘decuplet’ (ten-fold multiplicity). $SU(2)$ flavor (isospin) particle multiplets are located along straight horizontal lines within the $SU(3)$ flavor multiplet planes.

The requirement that quarks form antisymmetric bound states leads to classification in these two spin-flavor configurations of spin $\frac{1}{2}^+$ and $\frac{3}{2}^+$, respectively, and thus when symbols are repeated, the excited state is the higher spin state. States with positive intrinsic parity (upper index ‘+’) are shown, since negative parity is associated with intrinsic angular-momentum excitation, or the presence of an additional particle component such as a gluon or, equivalently, a quark-antiquark pair. Therefore, generally such excited negative-parity states can decay rapidly into the more stable positive-parity states.

Moving up in the two ‘pyramids’, we replace at each ‘floor’ one of the strange quarks by a charmed quark, omitting the non-strange baryons.

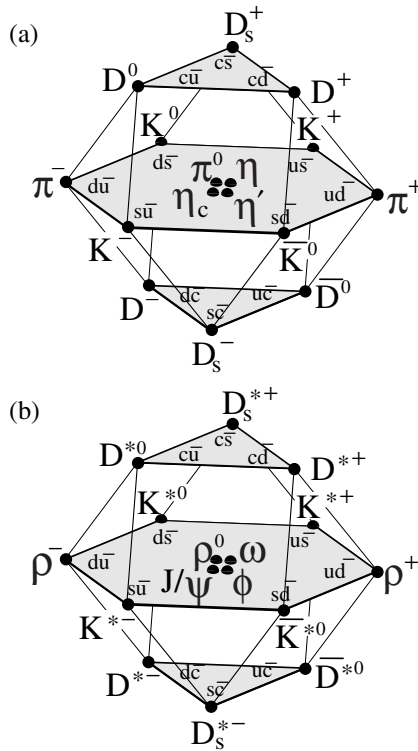


Fig. 2.2. Mesons (negative parity, superscript $-$): (a) pseudoscalar 0^- and (b) vector 1^- mesons, classified according to their valence-quark content.

quark component $s\bar{s}$; there is no pure spin-0 $s\bar{s}$ state. In the spin-1 octet, case $\phi^0 = s\bar{s}$ is a pure strange-quark pair state. Not considered in Fig. 2.2 are states containing bottom quarks:

$B = \pm 1$, bottom mesons: $B^+ = u\bar{b}$, $B^0 = d\bar{b}$, $\bar{B}^0 = \bar{d}b$, and $B^- = \bar{u}b$;
 $B = \pm 1$, $S = \pm 1$, bottom strange mesons: $B_s^0 = s\bar{b}$, and $\bar{B}_s^0 = \bar{s}b$; and
 $B = \pm 1$, $C = \pm 1$, bottom charmed mesons: $B_c^+ = \bar{b}c$ and $\bar{B}_c^- = b\bar{c}$.

2.2 Strange hadrons

For the physics of interest in this book, a particularly important family of particles consists of those which contain strange quarks. Since we will address these particles by implying some of their particular properties, we will summarize in the following their key features, and we comment on the experimental methods for their detection. A similar comment applies to heavier flavors (charm and bottom), and we also present a sample of these particles below.

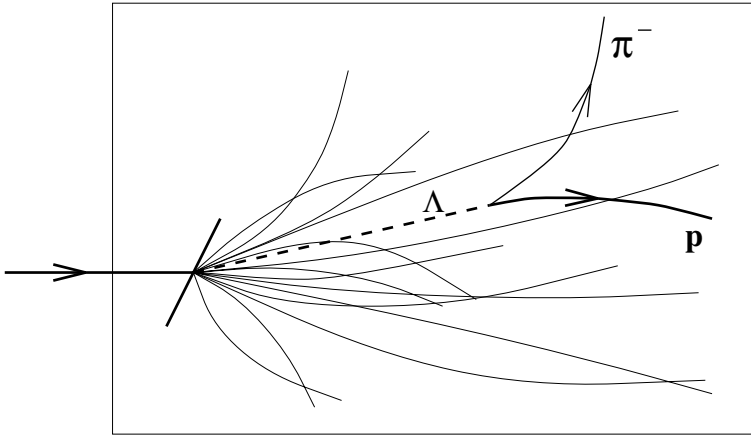
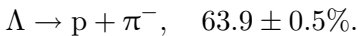


Fig. 2.3. A schematic representation of the Λ -decay topological structure showing as a dashed line the invisible Λ and the decay 'V' of the final-state charged particles. Tracks of other directly produced charged particles propagating in a magnetic field normal to the plane of the figure are also shown.

• **Hyperons** $Y(qqs)$ and $\bar{Y}(\bar{q}\bar{q}\bar{s})$

Sometimes all strange baryons are referred to as hyperons. We prefer to use this term for singly strange baryons.

— The isospin singlet lambda, $\Lambda(uds)$, is a neutral particle of mass 1.116 GeV that decays weakly with proper path length $c\tau = 7.891 \pm 0.006$ cm. The dominant and commonly observed decay is

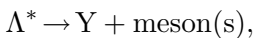


The decay of a neutral particle into a pair of charged particles forms a characteristic 'V' structure as shown in Fig. 2.3. The other important weak decay,



has only (hard-to-identify) neutral particles in the final state.

In addition to the $\frac{1}{2}^+$ ground state (positive parity, spin $\frac{1}{2}$: $\frac{1}{2}^+$), we encounter a $\frac{1}{2}^-$ resonance $\Lambda^*(1.405)$ and also a $\frac{3}{2}^-$ state $\Lambda^*(1.520)$. There is no 'stable' positive parity $\frac{3}{2}^+$ iso-singlet Λ . $\Lambda^*(1.520)$ has a remarkably narrow width $\Gamma = 15.6$ MeV, even though the hadronic decay into the $N\bar{K}$ channel is open. All Λ^* excited resonance states (13 are presently known, with mass below 2.4 GeV) decay hadronically into two principal channels:



Since the hadronic decays have free-space proper decay paths of 1–10 fm (widths $\Gamma = 16\text{--}250$ MeV), all these resonances can not be distinguished from the ground state of corresponding flavor content and contribute to the abundance of the observed ‘stable’ (on hadronic time scale) strange particles Λ and K . However, it is possible to measure their yields by testing whether the momenta of the expected decay products add to the energy–momentum product of a particle with the ‘invariant’ mass of the parent resonance.

The practical approach to the observation of Λ is to detect, in a tracking device, the (dominant) decay channel. The two final-state charged particles are pointing to a formation vertex remote from the collision vertex of projectile and target. The ancestor neutral particle should point to the interaction ‘star’ (see Fig. 2.3) and should have the correct mass and life span. This approach includes, in a certain kinematic region, the events which originate from the decay of K_s (see below). A well-established method of analysis of data allows one to distinguish the hyperon decay products from kaon decay products [211]. The procedure we describe in the following is named after Podolanski and Armenteros [208]. It exploits the difference between the phase-space distributions of the pair of particles produced.

The invisible neutral particle, reconstructed from the charged tracks forming the decay ‘V’, has a definitive line of flight, shown by the dashed line in Fig. 2.3. The magnitude of the transverse momentum q_{\perp} measured with reference to this line of flight is by definition the same for both produced, oppositely charged, particles. The longitudinal momentum $p_{\parallel}^+ \neq p_{\parallel}^-$ for each particle is dependent on a random angular distribution of decay products of charges $+$ and $-$. The relative p_{\parallel} asymmetry,

$$a = \frac{p_{\parallel}^+ - p_{\parallel}^-}{p_{\parallel}^+ + p_{\parallel}^-}, \quad (2.1)$$

can span the entire range $-1 < a < 1$ when the decay products have the same mass, as is the case for decay of kaons. When a proton is produced in Λ decay, this massive particle carries the dominant fraction of p_{\parallel} momentum and the event appears near $a \rightarrow 1$. Similarly, the $\bar{\Lambda}$ decay populates the domain $a \rightarrow -1$. Events appear around the clearly visible kinematic $q_{\perp}(a)$ lines shown in Fig. 2.4. For each decay of particles K_s , Λ , and $\bar{\Lambda}$, there is a clear domain where accidental misidentification of particles is impossible. e^+e^- -pair events produce a background found near to $q_{\perp} = 0$. The entire (q_{\perp}, a) plane is filled with events arising from accidental ‘V’s. Since the physical signal is highly concentrated along the kinematic lines seen in Fig. 2.4, the signal-to-noise ratio is very favorable. As a consequence, the measurement of production of neutral

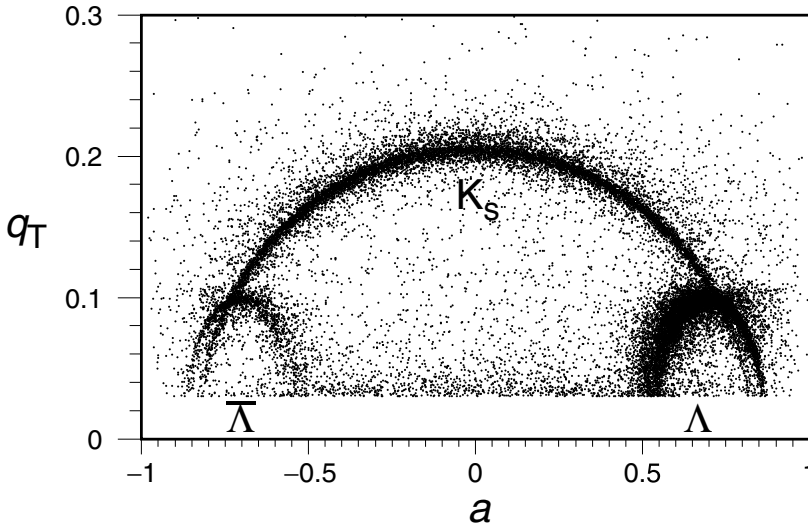


Fig. 2.4. The Podolanski–Armenteros representation of a particle-decay event: the transverse momentum q_T in a two-particle decay, as a function of the relative longitudinal momentum asymmetry a , see Eq. (2.1).

strange hadrons using Podolanski–Armenteros analysis is highly reliable.

— The isospin triplet uds , uus , dds , i.e., $\Sigma^0(1.193 \text{ GeV})$ and $\Sigma^\pm(1.189 \text{ GeV})$, varies in its properties. There is only one dominant decay channel for the Σ^- decay,

$$\Sigma^- \rightarrow n + \pi^-, \quad c\tau = 4.43 \pm 0.04 \text{ cm}.$$

Because there are two isospin-allowed decay channels of similar strength for the Σ^+ ,

$$\begin{aligned} \Sigma^+ &\rightarrow p + \pi^0, & 51.6\%, \\ &\rightarrow n + \pi^+, & 48.3\%, \end{aligned}$$

the decay path is nearly half as long, $c\tau = 2.4 \text{ cm}$. Σ^\pm have not yet been studied in the context of QGP studies, since they are more difficult to observe than Λ – akin to the Ξ decay (see below) there is always an unobserved neutral particle in the final state of Σ^\pm decay. Unlike Ξ decay, the kink that is generated by the conversion of one charged particle into another, accompanied by the emission of a neutral particle, is not associated with subsequent decay of the invisible neutral particle accompanied by a ‘V’ pair of charged particles; see Fig. 2.7 below.

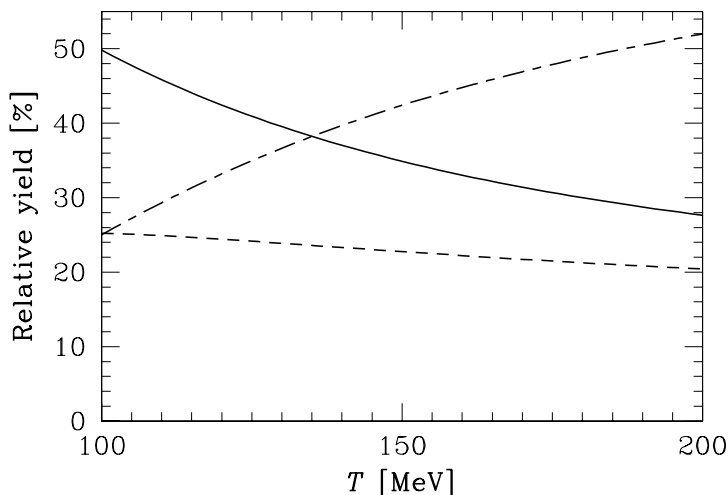


Fig. 2.5. The relative yields of the three dominant contributions to the final yield of Λ : direct production (solid line), Σ^0 contribution (dashed line), and $\Sigma^*(1385)$ contribution (chain line), as a function of T , the temperature of the hot source of these particles.

— The neutral $\Sigma^0(uds)$ undergoes a rapid electromagnetic decay:

$$\Sigma^0 \rightarrow \Lambda + \gamma + 76.96 \pm 0.02 \text{ MeV}, \quad c\tau = (2.2 \pm 0.2) \times 10^{-9} \text{ cm},$$

$$\tau = (7.4 \pm 0.7) \times 10^{-20} \text{ s}.$$

For the observer in the laboratory, this secondary Λ is practically indistinguishable from the direct production in the interaction vertex. Consequently, all measurements of Λ of interest for this book combine the abundances of Λ and Σ^0 , including all the higher resonances that decay hadronically into these states, in particular $\Sigma^*(1385)$.

As with Λ , there are several (nine) heavier Σ resonances known at $m \leq 2.4 \text{ GeV}$. When they are produced, all decay hadronically, producing \bar{K} , Λ , and Σ . Particularly important is the strong resonance $\Sigma^*(1385)$:

$$\Sigma^*(1385) \rightarrow \Lambda + \pi, \quad 88 \pm 2\%,$$

$$\rightarrow \Sigma + \pi, \quad 12 \pm 2\%.$$

Thus, $92 \pm 3\%$ of $\Sigma^*(1385)$ decays into Λ . Since the spin of $\Sigma^*(1385)$ is $\frac{3}{2}$, and its isospin is 1, the degeneracy of $\Sigma^*(1385)$ is six times greater than that of Λ . For this reason the final yield of Λ is in fact predominantly derived from decays of Σ^* , as is shown in Fig. 2.5, in which the chain line describes the partial contribution of Σ^* to the final yield of Λ . The solid line is the directly produced component, and the dashed line is the contribution of Σ^0 .

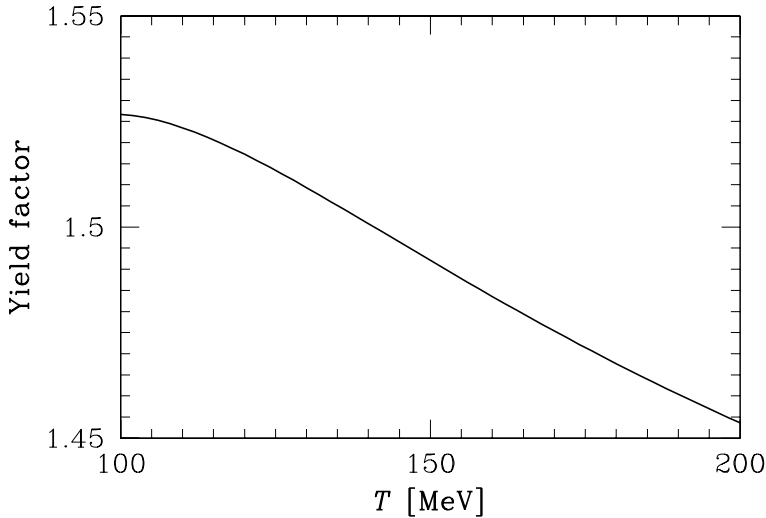


Fig. 2.6. The multiplicative factor allowing one to infer the total yield of qqs states from the observed yield of Λ as a function of T , the temperature of the hot source of these particles.

An important practical issue is the determination of the total yield of singly strange baryons (qqs), considering that we have available the observed yield of Λ . It is generally assumed that abundances of the three isospin-1 states Σ^+ , Σ^- and Σ^0 produced in relativistic nuclear collisions are equal. In the first instance, let us ignore the influence of $\Sigma^*(1385)$, which we introduce in the next paragraph. Considering the difference in mass between Λ and Σ , $\Delta m = 77$ MeV, and assuming that the relative abundance yield is appropriately described by the relation,

$$\frac{Y_{\Sigma^i}}{Y_{\Lambda}} = \left(1 + \frac{\Delta m}{m}\right)^{3/2} e^{-\Delta m/T}, \quad (2.2)$$

derived from the relative thermal phase-space size, Eq. (10.50c), one finds for a reasonable range of values $T = 160 \pm 15$ MeV, implied by thermal hadron production models, that the total yield of hyperons (qqs) is obtained by multiplying the experimentally observed yield of Λ by a factor $F_Y = 1.8$.

This estimate has to be modified in order to allow for the important role $\Sigma^*(1385)$ plays as a contributor to the production of Λ . In Fig. 2.6, we evaluate the yield factor F_Y allowing for the contributions of Σ^0 and $\Sigma^*(1385)$ to the yield of Λ , using thermal phase space, Eq. (10.51). There is very little variation with T in a wide range, $100 \text{ MeV} < T < 200 \text{ MeV}$, and we conclude that, for all practical purposes, one can use the yield factor $F_Y = 1.48 \pm 0.03$ to estimate the yield of singly strange

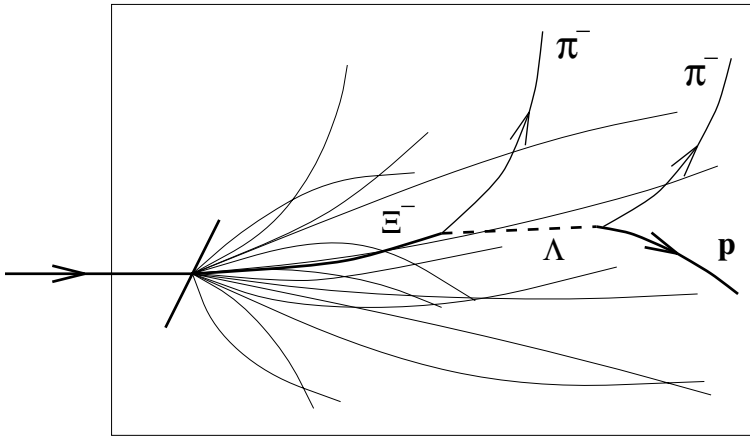


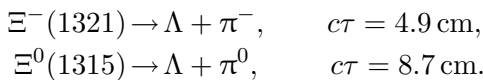
Fig. 2.7. A schematic representation of the topological structure of decay of Ξ^- showing as a dashed line the invisible Λ emerging from the decay kink and the decay ‘V’ of the final-state charged particles. Tracks of other directly produced charged particles propagating in a magnetic field normal to the plane of the figure are also shown.

baryons (qq s) from the observed yield of Λ . Naturally, this result holds for antibaryons as well. In many publications a slightly larger value, $F_Y = 1.6$, is applied.

At a smaller level the decays of multistrange Ξ and $\bar{\Xi}$ also contribute to the yield of Λ and $\bar{\Lambda}$, but this contribution is usually separated experimentally.

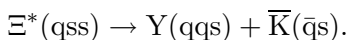
- **Cascades**, Ξ (qq s) and $\bar{\Xi}$ ($\bar{q}\bar{s}\bar{s}$)

The doubly strange cascades, Ξ^0 (uss) and Ξ^- (dss), are below the mass threshold for hadronic decays into hyperons and kaons, and also just below the weak-decay threshold for the $\pi + \Sigma$ final state. Consequently, we have one decay in each case:



The first of these reactions can be found in charged-particle tracks since it involves conversion of the charged Ξ^- into the charged π^- , with the invisible Λ carrying the ‘kink’ momentum. For Ξ^- to be positively identified, it is required that the kink combines properly with an observed ‘V’ of two charged particles identifying a Λ decay. This decay topology is illustrated in Fig. 2.7.

There are also several Ξ^* resonances known, which normally feed down in a hadronic decay into the hyperon and kaon abundances:



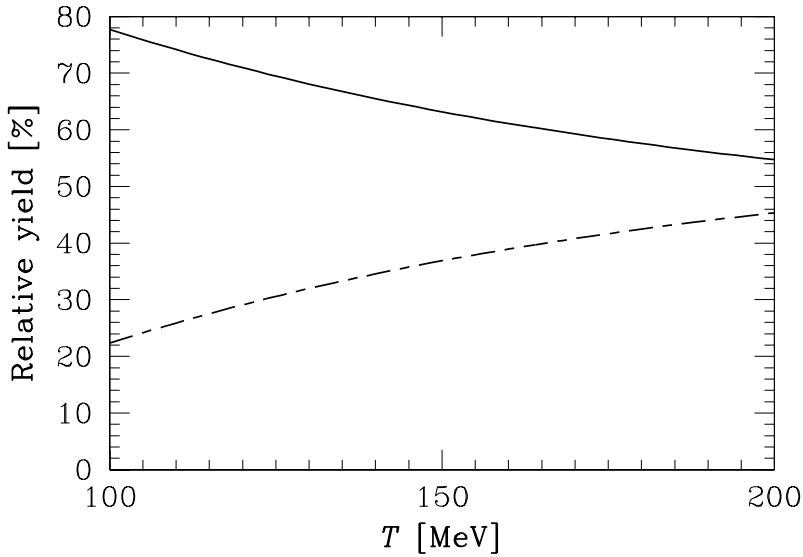
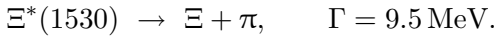


Fig. 2.8. The relative strength of the two dominant contributions to the final yield of Ξ : direct production (solid line), and $\Xi^*(1530)$ (chain line), as a function of T , the temperature of the hot source of these particles.

The main exception is the hadronic decay of the spin- $\frac{3}{2}$ recurrence of the spin- $\frac{1}{2}$ Ξ ground state:

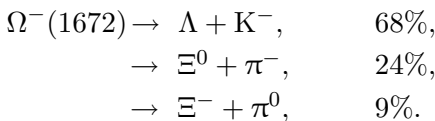


This relatively small width corresponds to $c\tau = 21$ fm and this decay occurs outside of the space-time region of hot matter.

Since the spin- $\frac{3}{2}$ state is populated twice as often as is the spin- $\frac{1}{2}$ ground state, its relative suppression due to the greater mass ($\Delta m \simeq 200$ MeV) is by a factor of 0.6, as is shown in Fig. 2.8. Despite this non-negligible decay contribution, the cascade spectra are, at high transverse momenta, the most representative among measured hadronic spectra of particles directly produced by the fireball of hot and dense matter.

• **Omegas**, $\Omega^-(sss)$ and $\bar{\Omega}^-(\bar{s}\bar{s}\bar{s})$

There are several primary weak-interaction decay channels leading to the relatively short proper decay path, $c\tau = 2.46$ cm:



The first of these decay channels is akin to the decay of the Ξ^- , except that the pion is replaced by a kaon in the final state. In the other two options,

after cascading has finished, there is a neutral pion in the final state, which makes the detection of these channels impractical. The $\Lambda + K^-$ decay channel is not unique for the $\Omega^-(1672)$ state; there is a $\Xi^*(1690)$ that also decays in the same way. However, this is a rapid hadronic decay that occurs in the interaction vertex and can be easily separated from the weak decay of the Ω .

The highest known resonance $\Omega^*(2250)$ is rather heavy. However, present experiments do not exclude the possibility of a light resonance, with a dominant electromagnetic decay, $\Omega^*(M^* < M_\Omega + m_\pi) \rightarrow \Omega + \gamma$. The presence of this resonance would greatly affect the theoretical expectations regarding the production of Ω and $\bar{\Omega}$ in heavy-ion interactions. The statistical degeneracy due to the high spin of such resonances could easily enhance their abundance, akin to the situation with the Ξ^* state we described above.

• **Kaons**, $K(q\bar{s})$ and $\bar{K}(\bar{q}s)$

— **Neutral kaons**, K_S and K_L ($m = 497.7$ MeV)

This is not the place to describe in detail the interesting physics of the short- and long-lived neutral kaons, except to note that both are orthogonal combinations of the two electrically neutral states ($d\bar{s}$) and ($\bar{d}s$). The short-lived combination K_S has $c\tau = 2.676$ cm and can be observed in its charged decay channel:

$$\begin{aligned} K_S &\rightarrow \pi^+ + \pi^-, & 69\%, \\ &\rightarrow \pi^0 + \pi^0, & 31\%. \end{aligned}$$

Care must be exercised to separate the K_S decay from Λ decay, since in both cases there are two, *a priori* unidentified, charged particles in the final state, making a ‘V’ originating from an invisible neutral particle; see Fig. 2.4.

The long-lived kaon K_L , with $c\tau = 1551$ cm, has not been studied in relativistic heavy-ion-collision experiments. Since both the K_L and the K_S arise from the time evolution of hadronically produced $K(d\bar{s})$ and $\bar{K}(\bar{d}s)$ their abundances are essentially equal.

— **Charged kaons**, $K^+(u\bar{s})$ and $K^-(\bar{u}s) \equiv \bar{K}^+$ ($m = 493.7$ MeV)

Charged kaons can in principle be observed directly, both in charged-particle-tracking devices and in magnetic spectrometers, since their mass differs sufficiently from those of the lighter π^\pm and the heavier proton/antiproton. Also, $K^\pm(494)$ decays with $c\tau = 371$ cm, with three principal channels:

$$\begin{aligned} K^+ &\rightarrow \mu^+ + \nu_\mu, & 63.5\%, \\ &\rightarrow \pi^+ + \pi^0, & 21.2\%, \\ &\rightarrow \pi^+ + \pi^+ + \pi^-, & 5.6\%. \end{aligned}$$

The last one, with three charged hadrons in the final state, can be used to identify charged kaons within tracking devices.

Considering the quark content, one sees that the average of the production of $K^+(u\bar{s})$ and $K^-(\bar{u}s)$ satisfies $\langle K_S \rangle \simeq 0.5(\langle K^+ \rangle + \langle K^- \rangle)$.

• **The ϕ -meson, $\phi(s\bar{s})$**

The vector ($J = 1$) meson ϕ is believed to be a ‘pure’ bound state of the strange-quark pair $\phi = s\bar{s}$. With mass 1019.4 MeV, it has a relatively narrow full width $\Gamma_\phi = 4.43$ MeV, since the decay into a pair of kaons is barely possible in free space. There are two open and relatively slow decay channels leading to the formation of pairs of leptons,

$$\begin{aligned} \phi \rightarrow e^+ + e^-, & \quad 0.03\%, & \quad \Gamma_{e^+e^-} = 1.32 \pm 0.05 \text{ keV}, \\ \phi \rightarrow \mu^+ + \mu^-, & \quad 0.025\%, & \quad \Gamma_{\mu^+\mu^-} = 1.3 \pm 0.2 \text{ keV}, \end{aligned}$$

allowing the determination of the number of ϕ -mesons emerging from the hadronic-interaction region. When absolute yields of particles are difficult to determine, one can compare, using the dilepton decay channel, the yield of ϕ with the yield of non-strange partner mesons $\rho(770)$ ($\Gamma_{e^+e^-} = 6.77 \pm 0.32$ keV) and $\omega(782)$ ($\Gamma_{e^+e^-} = 0.60 \pm 0.02$ keV).

2.3 Charm and bottom in hadrons

• **Onium-mesons, $c\bar{c}$, $b\bar{b}$ and $\bar{b}c$**

A brief summary of the physical properties of the three main onium states follows; the first three properties, mass (note the substantial systematic and statistical uncertainty in the mass of the B_c), lifetime and its inverse the width, are determined by measurement, followed by the binding energy with regard to dissociation into mesons, and the average size determined within heavy-quark potential models.

	$J/\Psi(c\bar{c})$	$B_c(\bar{b}c)$	$\Upsilon(\bar{b}b)$
Mass [MeV]	3097	$6400 \pm 390 \pm 130$	9460
τ [ps]	7.6×10^{-9}	$0.46 \pm 0.17 \pm 0.03$	12.5×10^{-9}
Γ [keV]	87 ± 5	1.4×10^{-6}	52.5 ± 1.8
Binding energy [MeV]	630	$\simeq 840$	1100
$\langle r \rangle$ [fm]	0.42	0.34	0.22

The spin-1 $J/\Psi(c\bar{c})$ has a partial width of 6% (per channel) projected into the experimentally observed lepton-pair channels $e^+ + e^-$, $\mu^+ + \mu^-$, i.e., $\Gamma_{\text{II}}^c = 5.26$ keV; the still narrower $b\bar{b}$ has $\Gamma_{\text{II}}^b = 0.3$ keV, which is 2.5% of the total width. We note that J/Ψ is produced very rarely in heavy-ion collisions, e.g., in Pb–Pb interactions at 158A GeV one J/Ψ is produced for each 3×10^6 mesons. Production of open charm has not been

measured but is at the level of 0.2–0.6 $c\bar{c}$ pairs per Pb–Pb interaction at 158A GeV. Thus, only one in about 2000 $c\bar{c}$ pairs produced emerges as a bound $J/\Psi(c\bar{c})$ state. The uncertainty in this estimate is at least a factor of two and depends on the centrality of the interaction. It is hoped that further experimental information will become available soon, allowing us to understand this ratio more precisely.

The excited state Ψ' has a yield five times smaller. There has not yet been a measurement of production of the other onium states in nuclear collisions.

In the LHC energy range, one can expect that the bound state of b-quarks, the upsilononium $\Upsilon(b\bar{b})$, will assume a similar role to that which is today being played, at SPS and RHIC energies, by J/Ψ .

The other heavy-quark bound state that is of interest is the $B_c(\bar{b}c)$. This quarkonium state is so rarely produced that it was not discovered until very recently [9, 10]. However, it has been studied extensively theoretically, and the currently reported mass, $M = 6.4 \pm 0.39 \pm 0.13$ GeV, is in good agreement with the theoretical quark-potential model expectations. The life span, $\tau \simeq 0.5$ ps, $c\tau \simeq 150$ μm , implies that the current silicon pixel detector technology allows one to distinguish the production vertex from the $B_c(\bar{b}c)$ decay vertex.

The conventional mechanism for production of $B_c(\bar{b}c)$ requires the formation of two pairs of heavy quarks in one elementary interaction, followed by the formation of a bound state. The probability of these three unlikely events occurring in one interaction is not large and hence neither is the relative predicted yield, $(B_c + B_c^*)/(b, \bar{b}) \simeq (3-10) \times 10^{-5}$ at $\sqrt{s_{NN}} = 200$ GeV [169]. This small value implies that ‘directly’ produced B_c (both in $J = 0$ and $J = 1$ channels B_c^* and \bar{B}_c^*) cannot be observed at the RHIC. On the other hand, an enhancement in production of this state is expected in the QGP-mediated recombination [239], which could lead to a measurable rate of production in nuclear interactions. Since the quark-recombination mechanism of production requires mobility of heavy color-charged quarks, observation of this new mechanism for the formation of this exotic meson would constitute another good signature of the deconfined QGP phase.

3 The vacuum as a physical medium

3.1 Confining vacuum in strong interactions

Theoretical interest in the study of relativistic heavy-ion collisions originates, in part, from the belief that we will be able to explore the vacuum structure of strong interactions and, in particular, the phenomenon of quark confinement. The picture of confinement can be summarized as